A fast radiative transfer model for simulating high-resolution absorption bands

Minzheng Duan and Qilong Min
Atmospheric Sciences Research Center, State University of New York at Albany, Albany, New York, USA

Jiangnan Li
Canadian Centre for Climate Modeling and Analysis, Meteorological Service of Canada, Victoria, British Columbia, Canada

Received 8 November 2004; revised 10 March 2005; accepted 18 April 2005; published 5 August 2005.

[1] A fast radiative transfer model has been developed for simulating high-resolution absorption bands. The first scattering radiance is calculated accurately by using the higher number of layers and streams for all required wave number grids. The multiple-scattering component is extrapolated and/or interpolated from a finite set of calculations in the space of two integrated gaseous absorption optical depths to the wave number grids: a double-k approach. The double-k approach substantially reduces the error due to the uncorrelated nature of overlapped absorption lines. More importantly, these finite multiple-scattering radiances at specific $k(\lambda_i)$ values are computed with a reduced number of layers and/or streams in the forward radiative transfer model. To simulate an oxygen A-band spectrum, 28 calculations of radiative transfer are needed to achieve an accuracy of 0.5% for most applications under all-sky conditions and 1.5% for the most challenging multiple-layer cloud systems (99% of spectrum below 0.5%). This represents a thousandfold time reduction in the standard forward radiative transfer calculation.

Citation: Duan, M., Q. Min, and J. Li (2005), A fast radiative transfer model for simulating high-resolution absorption bands, *J. Geophys. Res.*, *110*, D15201, doi:10.1029/2004JD005590.

1. Introduction

[2] The remote sensing community has for a long time recognized advantages in the oxygen A-band for retrieving atmospheric properties and constituents. Because oxygen is a well-mixed gas in the atmosphere, the pressure dependence of oxygen A-band absorption line parameters provides a vehicle for retrieving vertical profiles of atmospheric constituents from spectrometry of the oxygen A-band. The concept underlying oxygen A-band retrievals is the principle of equivalence [*Irvine*, 1964, 1967; *van de Hulst*, 1980], since the scattering properties of cloud and aerosol vary slowly and predictably with wavelength. In principle, high-spectral-resolution measurements (each individual line can be resolved) may be capable of discriminating atmospheric scattering from surface scattering, and thus provide a better remote sensing technique for retrieving vertical profiles of aerosols and clouds optical properties [*Stephens and Heidinger*, 2000; *Heidinger and Stephens*, 2000, 2002; *Stephens et al.*, 2005] (for a detailed review, see *Min et al.* [2004] and *Min and Harrison* [2004]). High-resolution ($\approx$0.5 cm^{-1}) oxygen A-band instruments were proposed for the Cloudsat and CALIPSO missions; unfortunately, both Cloudsat and CALIPSO A-band instruments were canceled because of difficulties with other portions of the satellite systems. Recently, the Orbiting Carbon Observatory (OCO) mission was approved, and a high-resolution instrument suite (O_2 A-band and two CO_2 bands) will be launched in 2007. We expect more high-resolution instruments in the future.

[3] Analyzing high-resolution spectral measurements requires radiative transfer calculations for simulating the spectrum. Each pixel of the measured high-resolution spectrum contains spectral responses from multiple absorption lines. Slight changes in instrument response function (e.g., wavelength registration and slit function) would change the measured spectrum significantly. To simulate a high-resolution spectrum, it is necessary to make radiative transfer calculations at much higher spectral resolution (in a line-by-line domain) and to convolve the calculated high-resolution spectrum with an adjusted instrument response function. Computing such a high-resolution spectrum is very time-consuming. A fast and accurate forward radiative transfer model is crucial to reduce the computational cost for operational retrievals. Various approximate techniques have been proposed to reduce the computing time in simulating oxygen A-band [*Stam et al.*, 2000; *Bennartz and Fischer*, 2000; *Min and Harrison*, 2004]. The basic methods that underlie those techniques are the correlated k-distribution for modest resolution (narrowband) applications and the principle of equivalence through photon path length distribution for high-resolution measurements. *Min and Harrison* [2004] outlined an approach for

0148-0227/05/2004JD005590$09.00

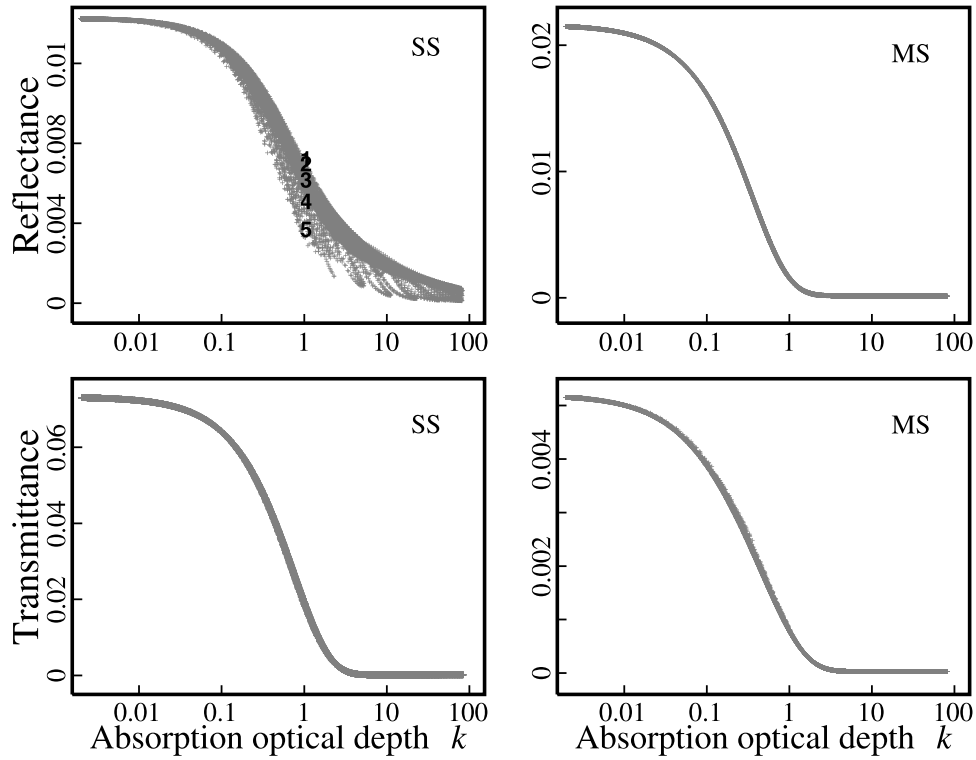

Figure 1. Single-scattering (SS) and multiple-scattering (MS) components of radiances as a function of oxygen absorption optical depths for oxygen A-band for a clear sky with background aerosol loading: The top panels are for the reflectance at TOA; the bottom panels are for transmittance at the surface. The solar zenith angle is 35°, view zenith angle is 0°, surface albedo is 0.02, and aerosol optical depth is set to be 0.08. See color version of this figure in the HTML.

simulating the oxygen A-band spectrum under clear-sky conditions. In their approach, the radiation from absorption and scattering processes of cloud and aerosol is split into the single- and multiple-scattering components: The first scattering component is computed accurately, and multiple-scattering (second order and higher) radiance is calculated approximately. In this paper, we extended and modified this technique to all-sky conditions on the basis of the equivalent theorem with a double-k distribution approach to account for the uncorrelated nature of overlapped absorption lines. In this double-k approach, two integrated absorption optical depths, the total absorption optical depth, k, and absorption optical depth from the top of the atmosphere to the scattering layer, k', are used to account for the vertical distribution of gaseous absorption in multiple-scattering media.

2. Methodology

2.1. Basic Steps for a Fast Forward Radiative Transfer Model

[4] A sensitivity study, based on the successive-order-of-scattering method [*Min and Duan*, 2004], shows that contributions of the first scattering to the total radiance are about 28, 50, and 95% for an atmosphere with total optical depth of 1 and single-scattering albedos of 1, 0.5 and 0.1, respectively. Figure 1 shows single- and multiple-scattering components of radiances across the oxygen A-band as a function of oxygen absorption optical depths (k) for the reflectance at the top of the atmosphere (TOA) and for the transmittance at the surface for a clear-sky case. Even for a case of cirrus cloud with optical depth of 2, shown in Figure 2, the ratio of the single-scattering component to the multiple-scattering component substantially decreases with an increase of absorption optical depth. In general, the calculation of single-scattering (the first order) radiance is accurate and fast, and most of the computational cost is spent on calculating multiple-scattering components. If the scattered radiation of higher orders can be obtained approximately to adequate accuracy with a fast approach, it would speed up calculations. Taking advantage of the equivalence theorem, the radiative transfer calculations can be transformed from wave number space to absorption optical thickness space (or k space). A finite set of calculations at some specific k values can be used to define the transformation, and then the radiances at all k values (or wave numbers) can be extrapolated and interpolated from the transformation relation [*Min and Harrison*, 2004]. This approach is to define a photon path length distribution from a finite set of k values implicitly and then apply the distribution to all wave number grids. The accuracy and efficiency of solving the radiative transfer equation also depend on the number of atmospheric layers and streams used in the calculations. A lower number of layers and streams would further

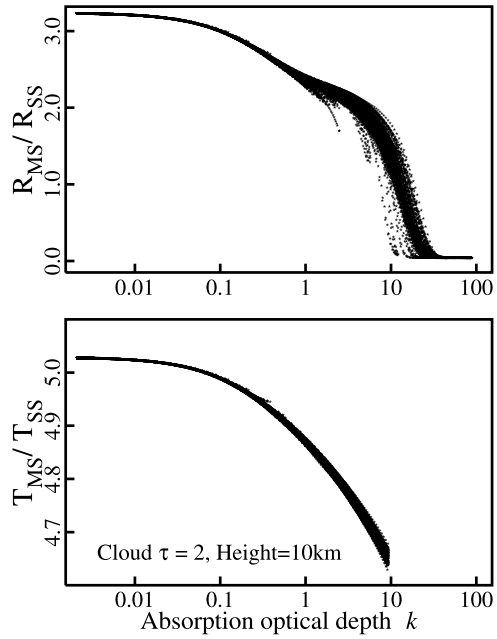

Figure 2. Ratio between single- and multiple-scattering (second order and higher) radiance: The top panel is for the reflectance at TOA; the bottom panel is for transmittance at the surface. The cloud is set between 9.335 and 10.05 km with optical depth of 2, and the geometry is the same as in Figure 1. See color version of this figure in the HTML.

reduce computational cost. On the basis of these principles, *Min and Harrison* [2004] proposed concrete steps for building a fast radiative transfer model, which are outlined in the following equations:

$$\begin{aligned} I &= I^{ss}(\lambda) + I^{ms}(\lambda) \\ &\approx I^{ss}\left[Z^h(p,t), P^h, \lambda\right] + I^{ms}\left[Z^h(p,t), P^h, \lambda\right] \\ &\approx I^{ss}\left[Z^h(p,t), P^h, \lambda\right] + I^{ms}\left[Z^l(p,t), P^l, \lambda\right] \\ &\approx I^{ss}\left[Z^h(p,t), P^h, \lambda\right] + I^{ms}\left\{F\left[Z^l(p,t), P^l, k(\lambda_i)\right]\right\} \end{aligned} \quad (1)$$

where Z is the optical properties of the atmosphere as a function of pressure and temperature. P is the phase function of that layer. *ss* and *ms* stand for single and multiple (second order and above) scattering, respectively. h and l represent higher and lower number of layers and streams, respectively. F is the transform function between wave number space and k space, defined from a finite set of $k(\lambda_i)$. The single-scattering radiance is accurately calculated by using the highest number of layers and streams for all required wave number grids. The multiple-scattering components are calculated in a small set of k values in k space to define the transformation function that transforms multiple-scattering components from k space. More importantly, these finite multiple-scattering radiances at specific $k(\lambda_i)$ values are computed with a reduced number of layers and/or streams in a forward radiative transfer model. These aspects of simplification for multiple-scattering components will substantially reduce the computational time.

2.2. Characteristics of Absorption Lines in Oxygen A-band and a Double-*k* Approach

[5] The lines in the A-band are well fitted as Lorentzian in the lower atmosphere:

$$k_i = \frac{S_i}{\pi} \frac{\alpha_i}{(\nu - \nu_i - \delta_i)^2 + \alpha_i^2} \quad (2)$$

where

$$\alpha_i = \alpha_i^0 (P/P_o)(T_0/T)^n \text{ and } \delta_i = \delta_i^0 (\rho/\rho_o) \quad (3)$$

and S_i is the line intensity, ν_i is the line center wave number, α_i is the half width, and δ_i is the line shift for the ith line. α_i^0, δ_i^0, and ρ_0 are the half-width, line shift and atmospheric density at standard pressure (P_0) and temperature (T_0), respectively. The value of n is, generally, between 0 and 1/2. The temperature and pressure dependency of absorption coefficients is different from a line center to the wing of the line as

$$\begin{aligned} k_\nu &\sim (P/P_o)(T_0/T)^n \quad \text{when} \quad \nu - \nu_0 - \delta \gg \alpha_0 \\ k_\nu &\sim (P_0/P)(T/T_0)^n \quad \text{when} \quad \nu - \nu_0 - \delta \ll \alpha_0 \end{aligned} \quad (4)$$

Figure 3 shows the absorption optical depth spectrum in the oxygen A-band calculated by a line-by-line (LBL) model

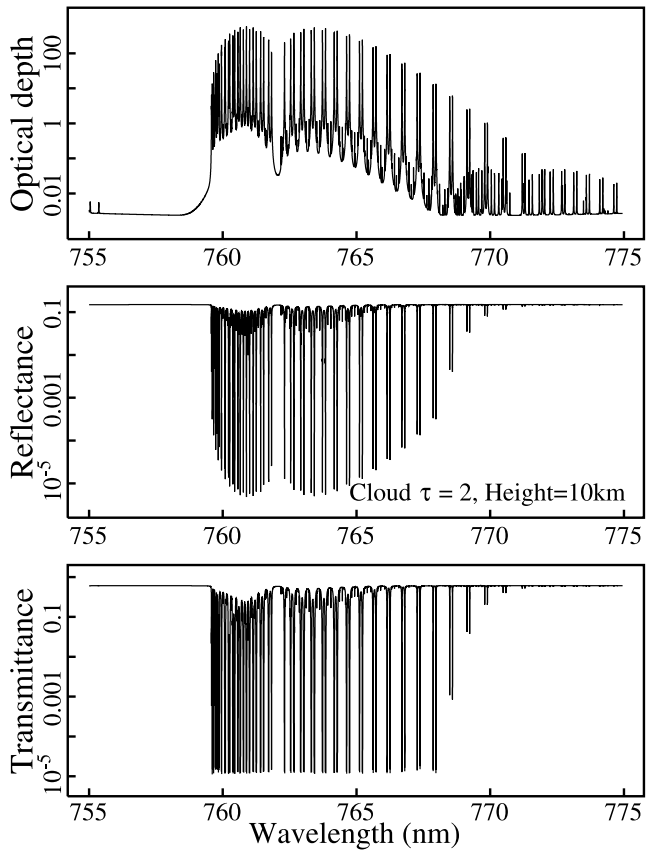

Figure 3. Absorption optical depth spectrum at resolution of 0.001 cm^{-1} and simulated benchmark spectra for a cirrus cloud case. See color version of this figure in the HTML.

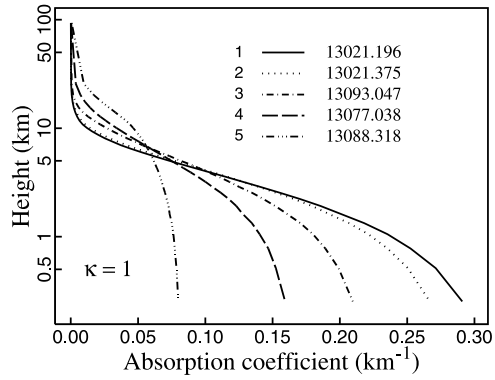

Figure 4. Vertical distributions of oxygen absorption at five wave numbers with the same total absorption optical depth. See color version of this figure in the HTML.

with a resolution of 0.001 cm^{-1} [*Clough et al.*, 1992; see http://www.rtweb.aer.com/lblrtm_frame.html]. The reflectance and transmittance spectra are calculated by a discrete ordinate radiative transfer (DISORT) model [*Stamnes et al.*, 1988] coupled with the LBL model. In both R and P branches, the lines at low rotational quantum numbers have strong absorption with centerline transmissions as low as 10^{-40} when observed at the surface. The lines in the wings of the band, with higher rotational quantum numbers, appear weak in absorption, because at atmospheric temperature few of the oxygen molecules populate these higher rotational states; consequently, the apparent strengths of the lines in the wings of the band are strongly temperature dependent because of Boltzmann statistics of the populations. In general, we have

$$S_i = S_i(T_0)\frac{T_0}{T}\exp\left[1.439E''\left(\frac{1}{T_0}-\frac{1}{T}\right)\right] \quad (5)$$

where E'' is the energy of the lower state of the transition, which increases significantly from the band center toward the wing region, while the normalized line strengths $S_i(T_0)$ decrease.

[6] Multiple absorption lines in the oxygen A-band overlap each other's wings, and the absorption coefficients of oxygen absorption lines strongly depend on the temperature and pressure of the atmosphere. As illustrated in Figure 4, for the same total absorption optical depth of 1, the vertical profiles of absorption optical depth significantly differ at different wave numbers. Vertical profiles at 13,021.196 and 13,021.375 cm^{-1} are different from each other since they are near the line center (13,021.29125 cm^{-1}) but on different sides of the line center. In contrast to the position of 13,021.375 cm^{-1} that is near its line center, 13,093.047 cm^{-1} is at the line wing far from its line center. Thus vertical profiles substantially differ as the temperature and pressure dependences of absorption coefficients are inverse. The vertical profiles at 13,077.038 and 13,088.318 cm^{-1} are different because of the different partitions of absorption between O^{16} and O^{18}, where most absorption comes from O^{18} absorption near its line center.

[7] Different absorption profiles of oxygen coupled with vertical distributions of scattering of aerosol and cloud result in substantially different radiation fields. The reflectances at TOA for the same total absorption optical depth

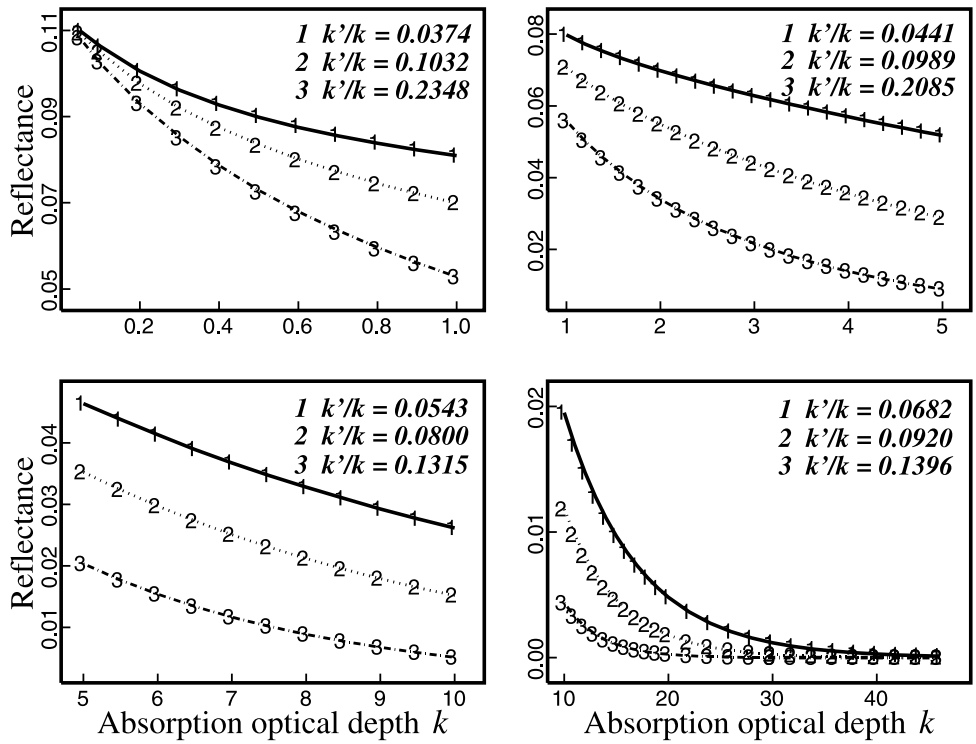

Figure 5. Comparison between the benchmark and interpolated reflectances at the TOA for four ranges of k at three different k' values. See color version of this figure in the HTML.

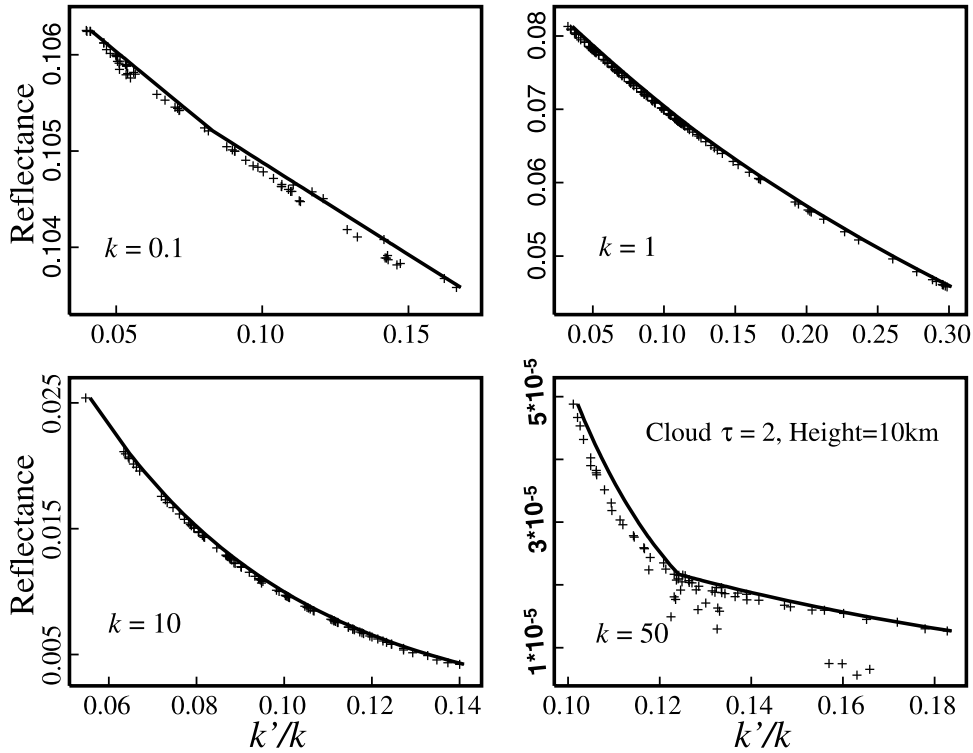

Figure 6. Comparison between benchmark and interpolated reflectances at the TOA as a function of $\xi(k'/k)$ for four specific k values. See color version of this figure in the HTML.

marked as numbers 1, 2, 3, 4, and 5 in Figure 1, related to the profiles shown in Figure 4, are substantially different (over 60%) because of different absorption profiles of oxygen. It illustrates that the uncorrelated nature of the atmosphere makes the correlation k-distribution method invalid in the high-resolution applications. To deal with this issue in a multiple-scattering regime, a double-k approach is proposed by introducing a second parameter, k'. The k'

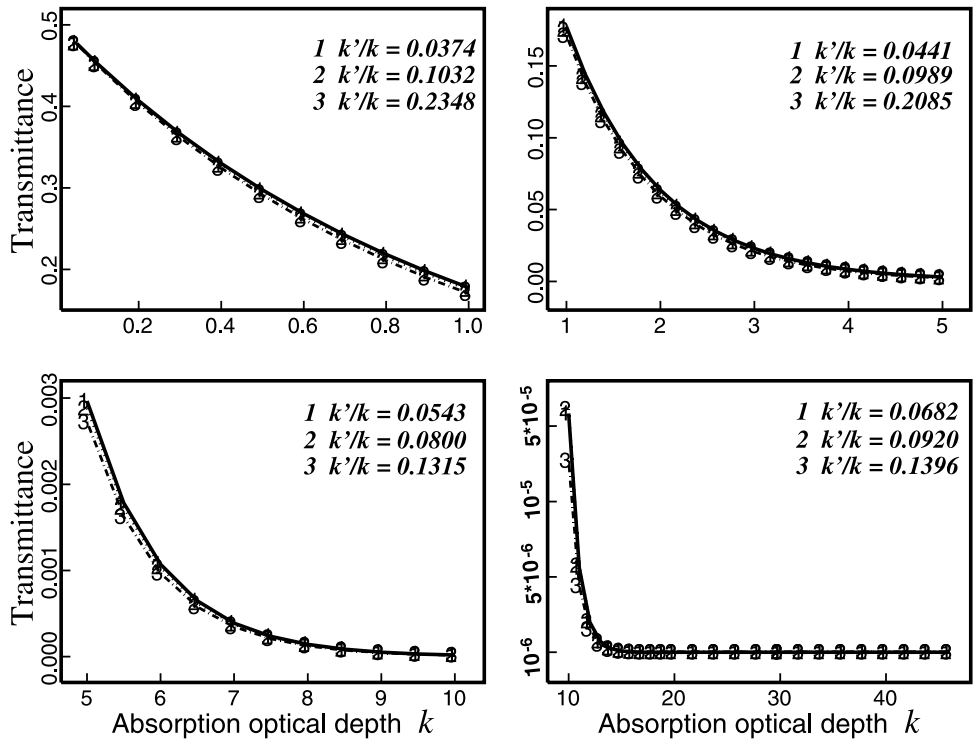

Figure 7. Comparison between the benchmark and interpolated transmittances at the surface for four ranges of k at three different k' values. See color version of this figure in the HTML.

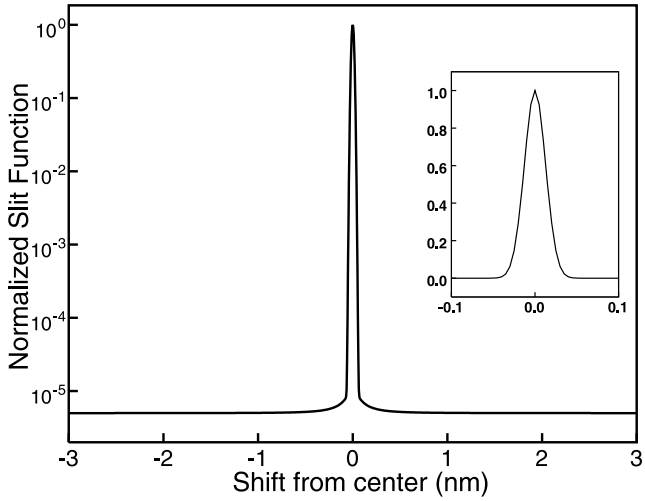

Figure 8. Assumed slit function in the simulations. See color version of this figure in the HTML.

parameter is the absorption optical depth from TOA to a layer where substantial scattering events take place. A new parameter, $\xi = k'/k$, represents the ratio of absorption depths. In this double-k approach, the multiple-scattering components in equation (1) can be written as

$$I^{ms}(\lambda) = I^{ms}\{F[Z^l(p,t), P^l, k(\lambda_i)]\} = I^{ms}\{F[k'(\lambda), k(\lambda)]\} = g(k) f_k(k'/k) \quad (6)$$

At the limits of strong and weak line approximations, the spectral transmittance can be written by a simple exponential function in terms of the generalized absorption coefficients [*Liou*, 1992]. In this fast approach, piecewise analytical functions are used to define $g(k)$:

$$g(k) = \begin{cases} \Gamma(\beta+1)/(k-\alpha)^{\beta+1} & k \in [0,1] \\ e^{-(a_1+b_1k+c_1k^2+d_1k^3)} & k \in [1,5] \\ e^{-(a_2+b_2k+c_2k^2+d_2k^3)} & k \in [5,10] \\ e^{-(a_3+b_3k)} & k \in [10,\infty] \end{cases} \quad (7)$$

When $k \in [0, 1]$, a simple analytical function is chosen, which implies a gamma function in photon path length distribution based on Laplace transfer from k space [*Harrison and Min*, 1997; *Min and Clothiaux*, 2003; *Lenoble*, 1985]. When $k > 1$, an exponential function is applied piecewise. Further, the function of $f_k(\xi)$ is defined as

$$f_k(\xi) = \begin{cases} \gamma_1 e^{-\beta_1 \xi} & \text{when} \quad \xi <= \xi_0 \\ \gamma_2 e^{-\beta_2 \xi} & \text{when} \quad \xi > \xi_0 \end{cases} \quad (8)$$

where ξ_0 is the average value of ξ for each fixed k. Equations (7) and (8) provide two-dimensional mapping for a given pair of double-k, k' and k. The coefficients in equations (7) and (8) can be easily solved by fitting accurately calculated multiple-scattering radiances. It is desirable to select k' at a layer where maximum events of scattering occur. Studies suggest that such a layer is generally located at scattering optical depth between 1.0 and 2.0 [*Duan and Min*, 2005]. For the case where the total scattering optical depth is greater than 2, a layer with scattering optical depth of 1.0 is selected to determine k' in the simulations. Otherwise, a layer with a half of the total scattering optical depth is selected for calculating k' values.

3. Results

[8] Speed is gained at the expense of accuracy, requiring optimization between these two aspects. Most spectrometers currently have absolute accuracy of 2% or worse. Therefore the goal of accuracy for this fast radiative transfer model is set to be 2% or better. To achieve this accuracy, the model needs to solve radiative transfer equation only 28 times to simulate the entire oxygen A-band (between 755 and 775 nm). The simplification represents a thousandfold reduction of standard LBL radiative transfer calculations. In the following discussion, the benchmark high-resolution spectra were simulated at spectral resolution of 0.001 cm^{-1} with a benchmark radiative transfer model that couples a LBL model with the radiative transfer solver, DISORT. In this benchmark model the standard atmospheric profile was used and divided into 34 vertical layers. The multiple scattering was computed with 48 streams.

3.1. Coefficient Fitting

[9] The coefficients in equations (7) and (8) are determined in the following procedures: (1) selecting k (ten,

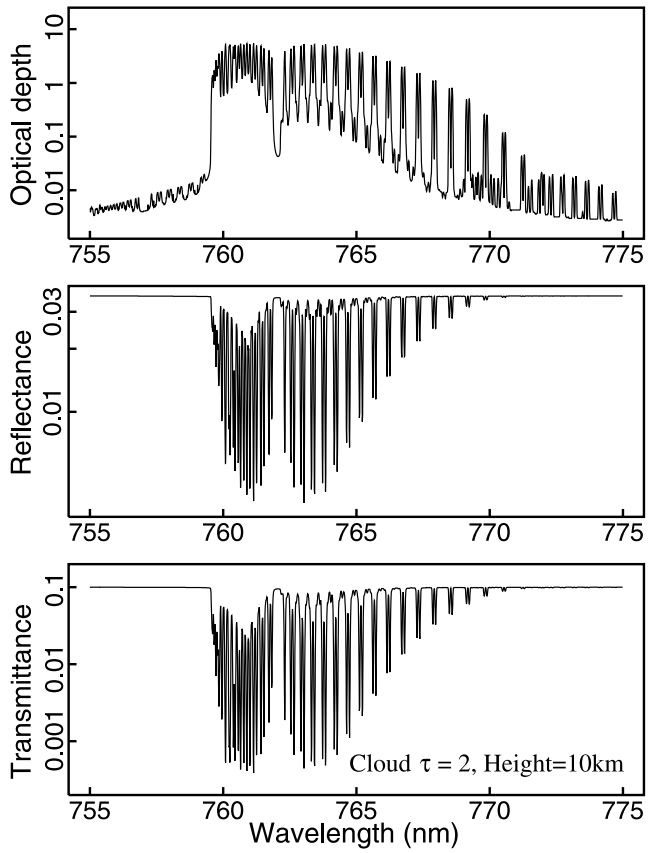

Figure 9. Absorption optical depth spectrum at the simulated instrument resolution and "observed" spectra for a cirrus cloud case. See color version of this figure in the HTML.

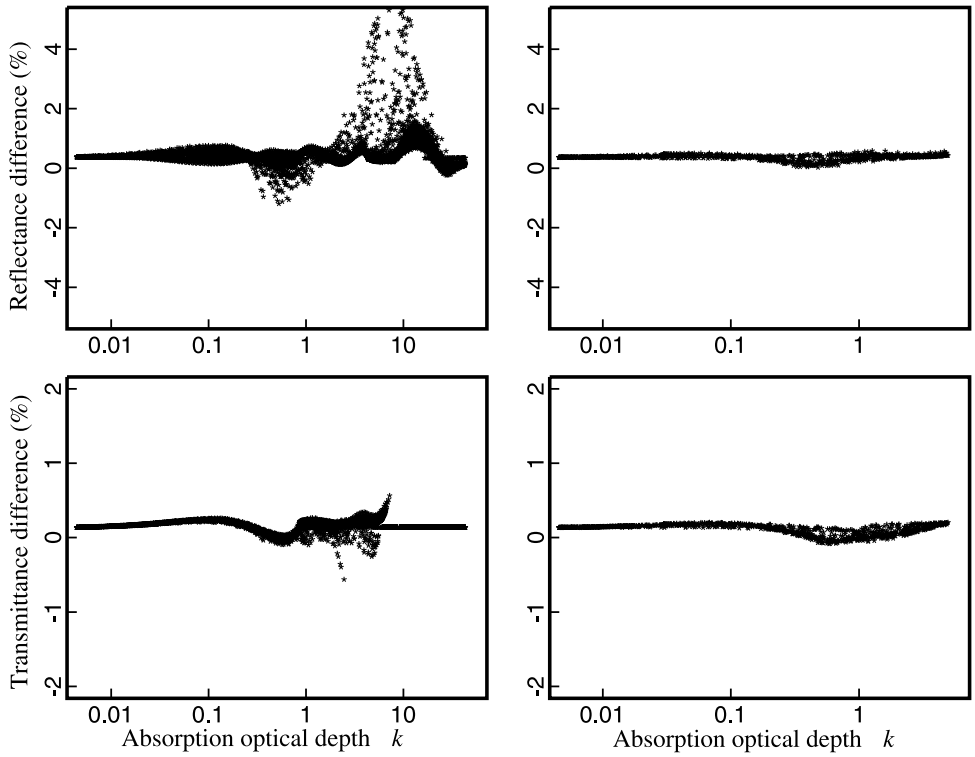

Figure 10. Differences between simulated spectra by the benchmark and fast radiative transfer models as a function of absorption optical depths for a cirrus cloud case: The two left plots are at high-resolution spectra (0.001 cm^{-1}); the two right plots are at instrument resolution after the convolution with instrument spectral response function. See color version of this figure in the HTML.

including $k = 0$ as the baseline) with an equal logarithmical increment of k; (2) selecting ξ_i (one for $k = 0$, and three otherwise, $i = -1, 0, 1$) on the basis of the dynamic range of k' for a given k; (3) computing the multiple-scattering radiance, $I^{ms}_{\xi_i}$, and normalizing $I^{ms}_{\xi_i}$ by $f = I^{ms}_{\xi_i}/I^{ms}_{\xi_0}$; (4) fitting equation (7) for $I^{ms}_{\xi_0}$ and equation (8) for f to determine all coefficients. For any wave number, the multiple-scattering component can be determined by equations (6)–(8) with corresponding values of k and $\xi = k'/k$. Figure 5 shows the comparison of the simulated benchmark results with interpolated reflectances based on equation (7) for four ranges of k at three different k' values. In this case (case 1 in the following case studies), a cirrus cloud with optical depth of 2 is located at 10 km (between 9.3 and 10.1 km), in addition to a background aerosol loading. The surface albedo is set to be 0.02. The differences between three k' values increase with absorption optical depths when k is not large, indicating the impact of vertical profile of absorption on cloud scattering process. When k is large, the differences are significantly reduced, as photons observed at TOA are dominated by single scattering. Figure 6 also illustrates that the piecewise exponential functions of equation (8) fit well for various values of ξ.

[10] Figure 7 shows the comparison for transmittances at the surface. Since all photons observed at the surface must experience at least one atmosphere of absorption, the perturbation of absorption due to different vertical profiles

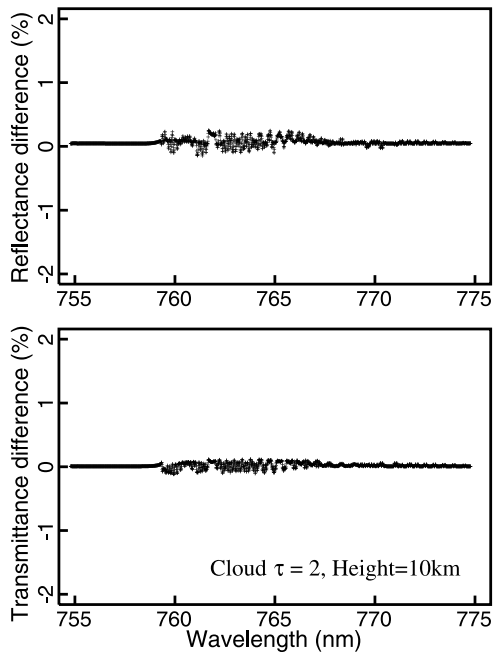

Figure 11. Differences of "observed" spectra as a function of wavelength for a cirrus cloud case. See color version of this figure in the HTML.

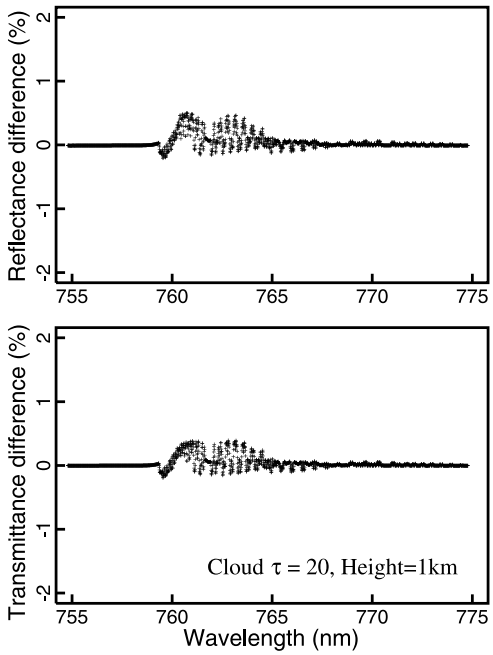

Figure 12. Same as Figure 11 but for a thick cloud case. See color version of this figure in the HTML.

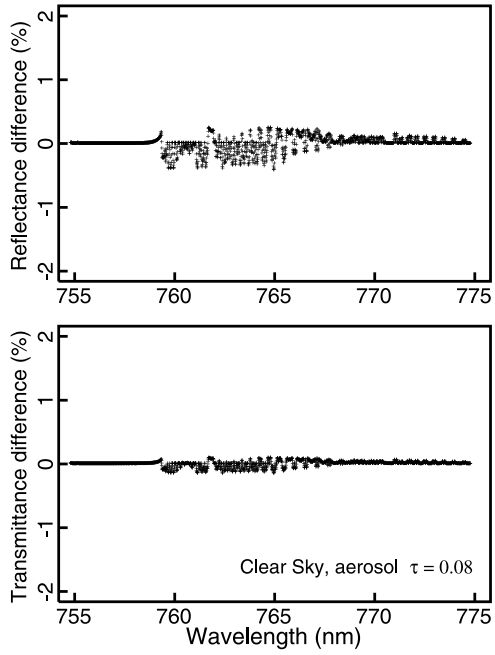

Figure 14. Same as Figure 11 but for an aerosol case. See color version of this figure in the HTML.

is a small fraction of total absorption. Therefore different vertical absorption profiles have small effect on transmittance. Again, the interpolated transmittances agree well with the benchmark results.

3.2. Case Studies

[11] Extensive testing of this fast radiative transfer model has been conducted. Four special cases will be discussed to illustrate accuracy of the fast radiative transfer model. The solar zenith angle is set to be 35 degrees, the surface is assumed to be Lambert with albedo of 0.02. Only nadir and zenith radiances are discussed in these case studies (radiances at other view angles show the similar accuracy). To mimic a real measurement, a realistic instrument slit function, shown in Figure 8, is used to convolve with the spectra calculated at the very high resolution of 0.001 cm^{-1}. This slit function is based on the measured slit function of high-resolution oxygen A-band and water vapor band spectrometer (HAWS) [*Min et al.*, 2004] and represents an instrument with full-width half-maximum (FWHM) of 0.5 cm^{-1} (0.03 nm) and out of band rejection of 5×10^{-6}.

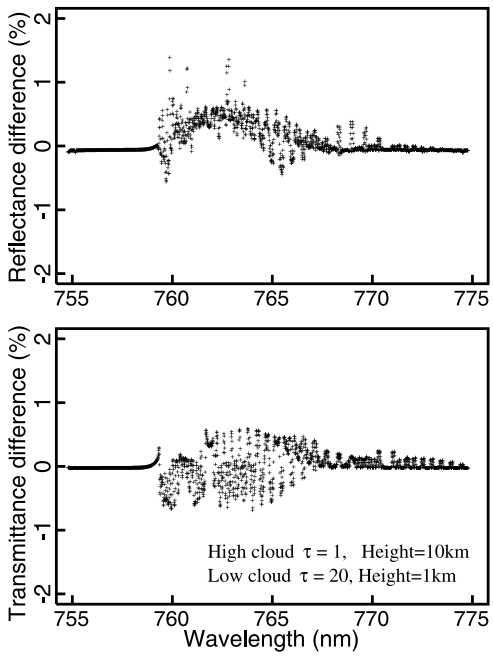

Figure 13. Same as Figure 11 but for a double-layer cloud case. See color version of this figure in the HTML.

[12] Case 1 is a cirrus cloud case with cloud optical depth of 2 at 10 km. The benchmark spectra (Figure 3) have been convolved with the slit function to yield the "observed" spectra at TOA and at the surface, shown in Figure 9. The maximum observable absorption optical depth, an indicator of instrument resolving power, is 5 for this instrument response function. Figure 10 shows the difference between the bench model and fast model results as a function of absorption optical depths: the two left plots for unconvolved spectra and two right plots for convolved spectra. The big differences for the reflectance spectrum without convolution occur at k values between 7 and 30 with magnitudes of 5% or so. However, the number of points with large errors are few, and the reflectances at these k values are small because of strong absorption. The reflectances at these k values make a small contribution to the observed radiance at a particular pixel when convolved with the instrument spectral response function. The differences for "observed" spectra, shown in the right panels of Figure 10, are reduced to less than 0.5%. Spectrally, as shown in Figure 11, the big differences occur at the centers of both branches where absorptions of oxygen are strong. The differences in transmittance are much smaller than that in reflectance.

[13] Case 2 is for a thi
(between 0.8 and 1.3 km).
to be 20 with effective ra
transfer model simulates a
the surface. Maximum diff
0.5% and 0.4% for reflec
respectively. The conclusio
2 that the accuracy of the f
any single cloud layer cas

[14] Case 3 is for a do
cloud (τ = 1) is located a
cloud (τ = 20) at 1 km. T
photons are not only sc
bounced between cloud
distribution is complicated
more pairs of k' and k to c
spectra simulated by this f
agree with the benchmark
in Figure 13. Only a few
1.5% occur at very large k
are very small. The errors
below the possible noise
measurements and errors associated with uncertainty of line parameters; thus they have limited impact on retrievals.

[15] Aerosol cases are much simpler than cloudy cases since scattering optical depths are small. In case 4, aerosol with optical depth of 0.08 is loaded into the atmosphere. Figure 14 shows the comparison of oxygen A-band spectra simulated by the benchmark model and by the fast radiative transfer model. The biggest differences for reflectance and transmittance spectra are less than 0.4% and 0.1%, respec-

accurately. (2) On the basis of the principle of equivalence, the calculation of multiple-scattering components can be transformed from wave number space to absorption optical depth space. (3) Because of multiple scattering, the radiation field is smoothed, i.e., there is a smoother distribution of photon path length, and the multiple-scattering radiances at absorption optical depths can be extrapolated and interpolated from a finite set of radiative transfer calculations at specific k values. (4) Given the same total absorption optical

depth k, the vertical profiles of each individual line are different because of the characteristics of absorption lines; thus the simple assumption of correlated k-distribution is invalid. (5) Accuracy of radiative transfer calculation depends on the numbers of vertical layers and streams. Therefore a fast and accurate radiative transfer model was developed by separating single- and multiple-scattering contributions and treating multiple scattering with a double-k approach.

[18] In the model, only 28 calculations of radiative transfer are needed to achieve an accuracy of 0.5% for most applications and 1.5% for the most challenging multiple-layer cloud systems (99% of spectrum below 0.5%). This represents a thousandfold time reduction in standard forward radiative transfer calculation for entire oxygen A-band spectrum. This approach is based on the sorting in the absorption optical depth space (total absorption optical depth, k, and absorption optical depth from TOA to the scattering layer, k'), which couples the absorption process with the scattering process in the atmosphere. The principles demonstrated here can be easily applied to other absorption bands, such as the H_2O and CO_2 absorption bands. Furthermore, this fast model builds upon a linear combination of single and multiple components and an interpolation with piecewise analytical functions. The derivatives (Jacobian) with respect to retrieved parameters can be easily obtained in this model.

[19] **Acknowledgment.** This research was supported by the Office of Science (BER), U.S. Department of Energy, through Atmospheric Radiation Measurement (ARM) grant DE-FG02-03ER63531 and through the Northeast Regional Center of the National Institute for Global Environmental Change (NIGEC) under cooperative agreement DE-FC03-90ER61010.

References

Bennartz, R., and J. Fischer (2000), A modified k-distribution approach applied to narrow band water vapour and oxygen absorption estimates in the near infrared, *J. Quant. Spectrosc. Radiative Transfer*, *66*, 539–553.

Clough, S. A., M. J. Iacono, and J.-L. Moncet (1992), Line-by-line calculation of atmospheric fluxes and cooling rates: Application to water vapor, *J. Geophys. Res.*, *97*, 15,761–15,785.

Duan, M., and Q.-L. Min (2005), A semi-analytic technique to speed up successive order of scattering model for optically thick media, *J. Quant. Spectrosc. Radiat. Transfer*, *95*, 21–32.

Harrison, L., and Q. Min (1997), Photon pathlengths from O_2 A-band absorption, in *IRS '96: Current Problems in Atmospheric Radiation, Proceedings of the International Radiation Symposium, Fairbanks, Alaska, 19–24 August 1996*, pp. 594–598, A. Deepak, Hampton, Va.

Heidinger, A. K., and G. L. Stephens (2000), Molecular line absorption in a scattering atmosphere. II: Application to remote sensing in the O_2 A-band, *J. Atmos. Sci.*, *57*, 1615–1634.

Heidinger, A. K., and G. L. Stephens (2002), Molecular line absorption in a scattering atmosphere. Part III: Pathlength characteristics and effects of spatially heterogeneous clouds, *J. Atmos. Sci.*, *59*, 1641–1654.

Irvine, W. M. (1964), The formation of absorption bands and the distribution of photon optical paths in a scattering atmosphere, *Bull. Astron. Inst. Neth.*, *17*, 266–279.

Irvine, W. M. (1967), Absorption bands and photon optical paths in a nonconservative scattering atmosphere, *Astrophys. J.*, *147*, 1193–1197.

Lenoble, J. (1985), *Radiative Transfer in Scattering and Absorbing Atmospheres: Standard Computational Procedures*, pp. 191–205, A. Deepak, Hampton, Va.

Liou, K. N. (1992), *Radiation and Cloud Processes in the Atmosphere: Theory, Observation, and Modeling*, Oxford Univ. Press, New York.

Min, Q., and E. E. Clothiaux (2003), Photon path length distributions inferred from rotating shadowband spectrometer measurements at the Atmospheric Radiation Measurements Program Southern Great Plains site, *J. Geophys. Res.*, *108*(D15), 4465, doi:10.1029/2002JD002963.

Min, Q.-L., and M. Duan (2004), A successive order of scattering model for solving vector radiative transfer in the atmosphere, *J. Quant. Spectrosc. Radiat. Transfer*, *87*, 243–259.

Min, Q.-L., and L. C. Harrison (2004), Retrieval of atmospheric optical depth profiles from downward-looking high-resolution O_2 A-band measurements: Optically thin conditions, *J. Atmos. Sci.*, *61*, 2469–2477.

Min, Q.-L., L. C. Harrison, P. Kiedron, J. Berndt, and E. Joseph (2004), A high-resolution oxygen A-band and water vapor band spectrometer, *J. Geophys. Res.*, *109*, D02202, doi:10.1029/2003JD003540.

Stam, D. M., J. F. De Haan, J. W. Hovenier, and P. Stammes (2000), A fast method for simulating observations of polarized light emerging from the atmosphere applied to the oxygen-A band, *J. Quant. Spectrosc. Radiative Transfer*, *64*, 131–149.

Stamnes, K., S.-C. Tsay, K. Jayaweera, and W. Wiscombe (1988), Numerically stable algorithm for discrete ordinate method radiative transfer in multiple scattering and emitting layered media, *Appl. Opt.*, *27*, 2502–2509.

Stephens, G., and A. Heidinger (2000), Molecular line absorption in a scattering atmosphere: I. Theory, *J. Atmos. Sci.*, *57*, 1600–1614.

Stephens, G. L., A. Heidinger, and P. Gabriel (2005), Photon paths and cloud heterogeneity: Toward an observational strategy for assessing the effects of 3D geometry on radiative transfer, in *Three-Dimensional Radiative Transfer for Cloudy Atmospheres*, edited by A. Marshak and A. Davis, Springer, New York, in press.

van de Hulst, H. C. (1980), *Multiple Light Scattering: Tables, Formulas, and Applications*, vol. 1, Elsevier, New York.

M. Duan and Q. Min, Atmospheric Sciences Research Center, State University of New York at Albany, 251 Fuller Road, Albany, NY 12203, USA. (dmz@asrc.cestm.albany.edu)

J. Li, Canadian Centre for Climate Modeling and Analysis, Meteorological Service of Canada, P. O. Box 1700, STN CSC, Victoria, BC, Canada V8W 2Y2.